Equilibrium between NO_3^- and NO_2^- in KNO_3–$NaNO_2$ melts: a Raman spectra study

Xianwei Hu (胡宪伟)[1,2*], Zongxin Yu (喻宗鑫)[1,2], Bingliang Gao (高炳亮)[1,2], Zhongning Shi (石忠宁)[1,2], Jiangyu Yu (于江玉)[1,2], and Zhaowen Wang (王兆文)[1,2]

[1]*School of Materials and Metallurgy, Northeastern University, Shenyang 110819, China*
[2]*Engineering Research Center for Process Technology of Nonferrous Metallurgy, Ministry of Education, Shenyang 110819, China*
[*]*Corresponding author: huxw@smm.neu.edu.cn*

Received April 6, 2014; accepted June 11, 2014; posted online August 26, 2014

We study ionic structure of KNO_3–$NaNO_2$ melts under air atmosphere by using Raman spectroscopy. Molar fraction of NO_3^- and NO_2^- is obtained and thermal stability of this kind of melts system is then analyzed. The results show that when the temperature is increased to a certain value, equilibrium between the decomposition of NO_3^- and the oxidation of NO_2^- exists in KNO_3–$NaNO_2$ melts. When temperature is higher than 644 K, the molar fraction of NO_3^- decreases a little with temperature increasing for the melts in which the initial fraction of KNO_3 is 90 wt%, but for the melts in which the initial fraction of KNO_3 is 10–80 wt%, the molar fraction of NO_3^- increases with temperature, and the increasing rate is slower for a higher initial fraction of KNO_3. Molar fraction of NO_3^- increment increases linearly with initial fraction of $NaNO_2$. The sample in which the initial fractions of $NaNO_2$ are 11.3 and 14.5 wt% under air atmosphere shows the best thermal stability at 762 and 880 K, respectively.

OCIS codes: 300.6450, 290.5860.
doi: 10.3788/COL201412.093001.

Molten mixture of nitrate and nitrite has wide application as heat carrier in heat transfer and thermal storage industry and has been studied in the literature with recent reviews published[1–4]. Physicochemical properties, such as liquidus temperature, heat capacity, thermal stability, vapor pressure, and high-storage density are very important for this kind of melts for providing the basis for choice of composition and temperature. It is well known that the melts' properties are the external representation of their internal structure. Therefore, it is important to study the structure of nitrate and nitrite melts.

Raman spectroscopy is one of the important tools in the field of research on the structure of crystal, and with related technology progresses, it is also used in the study on structure of glass[5] and liquid[6]. Raman spectra studies on nitrate, nitrite, and the pertinent mixture are reported in previous literature. James *et al.*[7–10] researched the Raman spectra of molten nitrate of monovalent metals, such as $CsNO_3$, $RbNO_3$, KNO_3, $NaNO_3$, $TlNO_3$, $LiNO_3$, and $AgNO_3$. In their studies, interactions among different ions were emphatically analyzed and some binary systems were also involved. Clarke[11] thought that the structure of molten nitrate of monovalent metals was similar to solid through his Raman spectra study.

Toshiko *et al.*[12] also carried out a Raman spectra study on molten $LiNO_3$, $NaNO_3$, KNO_3, $RbNO_3$, $CsNO_3$, $AgNO_3$, and $TlNO_3$. In their study, vibrational law of NO_3^- and the effect of cationic kinds were mainly focused. Sakai *et al.*[13] investigated the interactions among ions in molten nitrate–nitrite system by visible and UV Raman spectroscopy, results indicated that the interactions among anions were small. Lieth *et al.*[14] studied the orientational disorder of NO_2^- in molten $NaNO_2$ by Raman spectroscopy.

Berg *et al.*[15] revised the $NaNO_3$–$NaNO_2$ phase diagram on the basis of Raman spectroscopy and differential scanning calorimetry study. Gao *et al.*[16] recorded the Raman spectra of KNO_3–$NaNO_2$–$NaNO_3$ mixture. The change law of bond length and angle of NO_3^- and NO_2^- were analyzed and the effect of $NaNO_3$ was studied.

However, in the above mentioned studies, there was no quantitative analysis involved. In a molten mixture of nitrate and nitrite, the equilibrium between NO_3^- and NO_2^- exists, and the properties such as capacity (energy density) and thermal conductivity are closely related to the relative concentrations of various ions. In fact, there have been quantitative studies of melts structure by Raman spectroscopy on fluoride-based molten salt system[17–20]. In the present study, anionic equilibrium composition in KNO_3–$NaNO_2$ melts was analyzed at different conditions by Raman spectroscopy. The results are hoped to find application in interpreting the change law of melts properties, comparing the thermal stability of the melts with various compositions and then providing theoretical guidance for industrial practice. It should be noted that the atmosphere affected the thermal stability of $NaNO_3$–KNO_3–$NaNO_2$ mixture significantly[21]. Considering the atmosphere in

practical application, Raman spectra were scanned under air atmosphere.

All chemicals were dried at 423 K for 24 h to remove water. In order to get the required composition, 15 g of salt mixture was mixed in an agate mortar in a Mbraun MB200B glove box, and then premelted to mix well in a quartz crucible. The cooled sample was ground in an agate mortar, too. About 0.1 g of the ground sample was taken for Raman spectra recording.

A Spectra-Physics 177-G1205 Ar^+ laser (20 mW, 487.97 nm) was used to generate the exciting laser and an Olympus micro objective (50×0.50) was used for observing the samples. Raman spectra were recorded by a Horiba Jobin Yvon LabRAM HR 800 Raman spectrometer accumulating for 30 s two times. The slit opening was set as 300 μm during the recording process.

The schematic view of the micro-furnace is shown in Fig. 1. The base and pillar were made of copper and aluminum, respectively. The pillar was connected to the main body by threaded connection. The main body consisted of two copper parts. They were connected by threaded connection and cooling water was passed through them. In the cavity of the furnace, a corundum tube with an external thread for the platinum wire providing heat wound around was placed. Sample was placed in the quartz crucible. A Guolong TCW-32B temperature controller connected to a Pt-$PtRh_{10}$ type thermocouple in contact with the bottom of the crucible was used to control the temperature. All of the Raman spectra were scanned under air atmosphere.

In a molten mixture of nitrate and nitrite, it takes a certain time for the concentrations of NO_3^- and NO_2^- to attain equilibrium under air atmosphere[22]. Therefore, the effect of holding time on the relative concentrations of NO_3^- and NO_2^- was first investigated and the sample in which the initial fraction of KNO_3 was 10 wt% was chosen as the test case.

Raman spectra of 10 wt% KNO_3–90 wt% $NaNO_2$ of different holding times under air atmosphere at 540 and

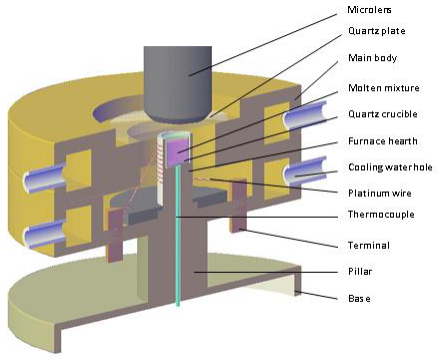

Fig. 1. Construction of the micro-furnace.

644 K are shown in Fig. 2. Baseline of some spectra has been corrected but no smoothing procedure was applied.

In the spectra shown in Fig. 2, v_1 characteristic band of NO_3^- and NO_2^- located at 1052 and 1327 cm^{-1} respectively are observed, and the other bands in the spectra are also assigned to other vibration modes of NO_3^- or NO_2^-[7,14]. There is no characteristic band caused by other species and this is in accordance with Ref. [23].

Values of the maximal height of the peak, the position of the maximum, and the bandwidth at half height for each characteristic band were obtained by fitting the bands to a summation of Gauss and Lorentzian's equation through the "peak searching and fitting" option of LabSpec software.

From the Raman spectral data, one can quantify the mixture sample[24]. The concentration of one kind of complex is proportional to the intensity of its corresponding characteristic peak, and the proportional coefficient is called scattering coefficient[25], which is affected by many factors, such as spectrometer verticality, laser power, optical collection system efficiency, and sample refractive index. Therefore, if the quantitative calculation is carried out on that basis, there will be large

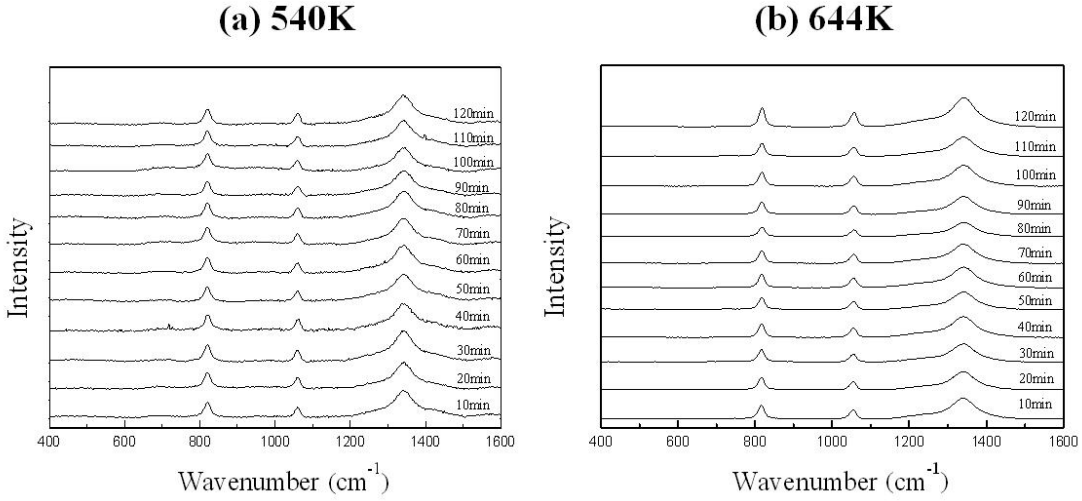

Fig. 2. Raman spectra of 10 wt% KNO_3–90 wt% $NaNO_2$ under air atmosphere of different holding times.

error. Another quantitative analysis method is based on the use of calibration curve of Raman intensity versus complex concentration, which is usually used in the Raman spectra study of the aqueous solution system[26]. Unlike the aqueous solution, in molten salt mixtures, the composition is shifted from the initial, and some species exist only in the molten state but not in the solid state. However, in the same spectrum, the intensity ratio between two different characteristic peaks is proportional to the concentration ratio between the corresponding complexes for the same optical conditions. Therefore, in the present study, the following equation is satisfied:

$$I = k\frac{n_3}{n_2}, \tag{1}$$

where I is the intensity ratio between v_1 characteristic peaks of NO_3^- and NO_2^-, k is the scattering coefficient ratio of NO_3^- and NO_2^-, and n_3 and n_2 are molar fractions of NO_3^- and NO_2^-, respectively.

Relationship between the value of I and the holding time at different temperatures is shown in Fig. 3. At 540 K, the sample just melted. It can be seen from Fig. 3 that the relative concentration of NO_3^- and NO_2^- at 540 K is almost constant. In fact, the decomposition of NO_3^- and oxidation of NO_2^- occur only after the melting of the mixture of nitrate and nitrite[22]. Therefore, it is thought that when the mixture just melts, the concentration ratio between NO_3^- and NO_2^- remains the same as the solid state.

Curve of 644 K in Fig. 3 shows that when the holding time increases, the equilibrium between NO_3^- and NO_2^- shifts to the NO_3^- side. That is, the concentration of NO_3^- increases, and only 30 min after melting of the mixture, the concentration ratio between NO_3^- and NO_2^- increases slowly with the holding time. Therefore, in the following experiments, the spectra will be scanned when the molten salts have had equilibration time of 30 min at every experimental temperature. During the selection of the holding time, the effect of volatilization is also considered. That is the probable cause of the slow increase in the intensity ratio after 30 min.

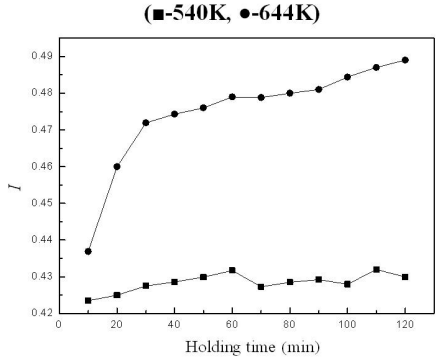

Fig. 3. Curve of I versus holding time in molten 10% KNO_3–90% $NaNO_2$.

Raman spectra of KNO_3–$NaNO_2$ under air atmosphere at different temperatures are shown in Fig. 4. Baseline of some spectra has also been corrected as required. The characteristic bands in the spectra in Fig. 4 were also fitted to a summation of Gauss and Lorentzian equation and the value of the related parameters was obtained. The fitting results indicate that characteristic bands show red-shift and the width of the bands increases with increasing temperature. That is universal in the melts because higher temperature leads to stronger atomic thermal motion and weaker interaction between atoms, which cause larger interatomic distance and bond angle. Moreover, high temperature will increase the disorder degree of the melts.

According to Eq. (1) and the total concentration of N elements in the melts, one can calculate the values of n_3 and n_2 by knowing the value of the intensity ratio between the two characteristic peaks. The above method has been used to calculate the concentrations of Al-F complex in molten aluminum electrolyte[20].

As stated above, in the present study, when the sample has just melted, the molar fraction of NO_3^- and NO_2^- is thought to be same as the corresponding initial molar fraction. Thus, value of k for each composition can be obtained prior to equilibrating at higher temperature. Then, the molar fraction ratio between NO_3^- and NO_2^- at different temperatures on that basis can be obtained. Molar fraction of NO_3^- for different initial compositions is shown in Fig. 5.

From Fig. 5, one can find that at temperature lower than 644 K, the concentration of NO_3^- is constant. However, when the temperature is higher than 644 K, for the melts in which the initial concentration of KNO_3 is 90 wt%, the concentration of NO_3^- decreases a little with temperature. Meanwhile, for all the other initial concentrations of KNO_3, the concentration of NO_3^- increases with temperature. Furthermore, the concentration of KNO_3 increases more rapidly for lower initial concentration of KNO_3.

It is thought that when the temperature is lower than 644 K, there is no decomposition of NO_3^- or oxidation of NO_2^-, and the evaporation rate is low. The molar fraction of NO_3^- and NO_2^- remains constant. But when the temperature is above 644 K, NO_2^- begins to be oxidized to NO_3^-. Thus, the equilibrium between NO_3^- and NO_2^- is easy to shift to the NO_3^- side for low initial concentration of KNO_3, and NO_3^- increases rapidly. For melts with higher initial concentration of KNO_3, molar fraction of NO_3^- increases more slowly. When the initial concentration of KNO_3 is 70 wt%, the molar fraction of NO_3^- is almost unchanged with temperature, as the initial concentration of NO_3^- is high and the oxidation of NO_2^- appears to be inhibited.

When the initial concentration of KNO_3 is 90 wt%, there is almost no oxidation of NO_2^-. When the temperature increases to the decomposition temperature of NO_3^-, the equilibrium between NO_3^- and NO_2^- shifts to the NO_2^- side, and for this the initial concentration of

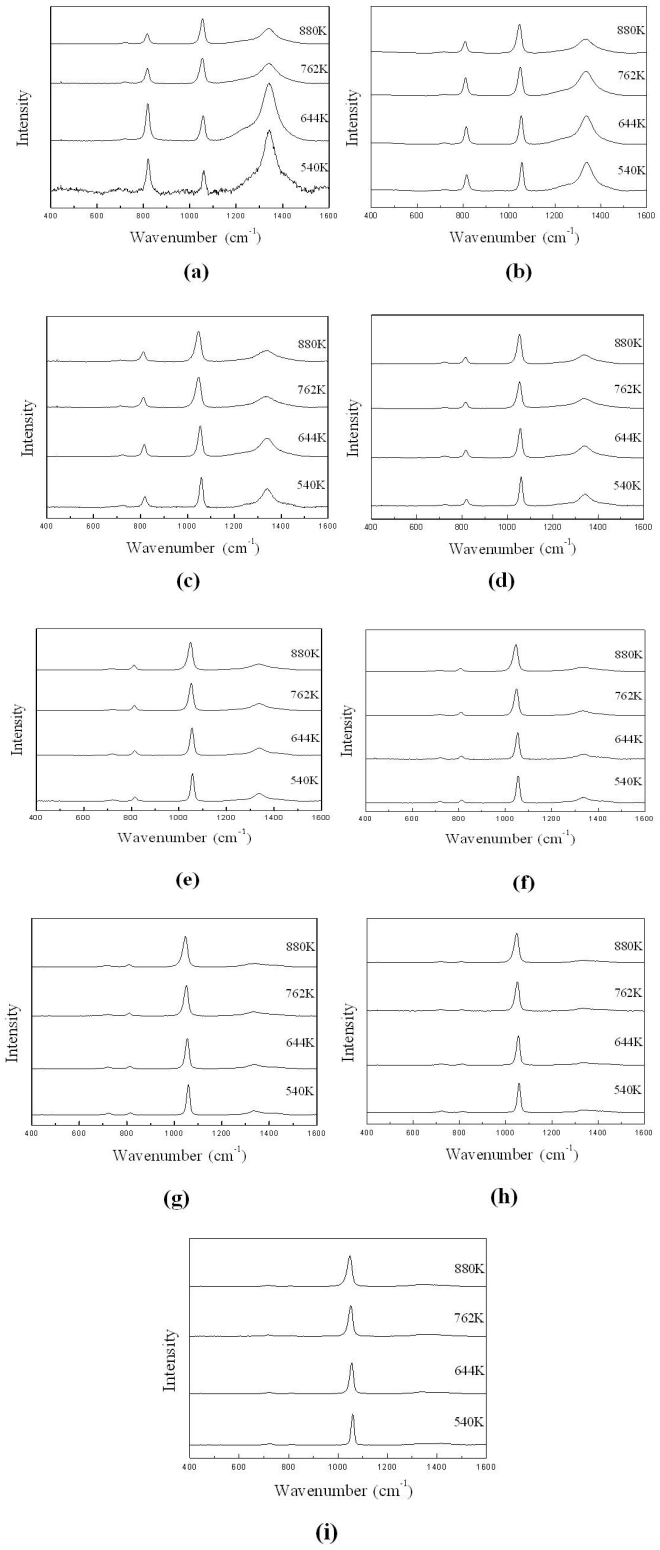

Fig. 4. Raman spectra of KNO_3–$NaNO_2$ melts under air atmosphere. KNO_3 concentration: (a)10, (b) 20, (c) 30, (d) 40, (e) 50, (f) 60, (g) 70, (h) 80, and (i) 90 wt%.

NO_2^- is low. Therefore, the molar fraction of NO_3^- decreases a little at the highest temperature.

In order to investigate the thermal stability of KNO_3–$NaNO_2$ melts, relationship between molar fraction

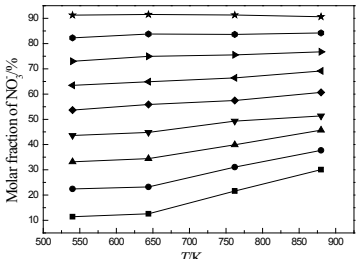

Fig. 5. Molar fraction of NO_3^- in KNO_3–$NaNO_2$ melts.

increment of NO_3^- (the difference between molar fraction of NO_3^- in the melts and initial) and initial mass fraction of $NaNO_2$ was examined. The relationship curves at 762 and 880 K are shown in Fig. 6.

Figure 6 shows that molar fraction increment of NO_3^- increases with initial mass fraction of $NaNO_2$. When the initial mass fraction of $NaNO_2$ is relatively low, the high-temperature equilibrium between NO_3^- and NO_2^- shifts to the NO_2^- side, so the concentration of NO_3^- is lower than its initial concentration, and when the initial mass fraction is higher than a certain value, the equilibrium shifts to the NO_3^- side, so the concentration of NO_3^- is higher than its initial concentration.

The curves shown in Fig. 6 are basically linear, and the linear equations are obtained by fitting the data points in Fig. 6.

$$\Delta X = -1.34 + 0.12m\,(762\ \mathrm{K}), \tag{2}$$

$$\Delta X = -3.35 + 0.23m\,(880\ \mathrm{K}), \tag{3}$$

where ΔX is the molar fraction increment of NO_3^- in percentage and m is the initial mass fraction of $NaNO_2$ in percentage.

In Eq. (2), when ΔX is equal to 0, the value of m is calculated to 11.3 wt%. In this case, the concentration of NO_3^- and NO_2^- is equal to the initial value, and the thermal stability is thought to be the best in that composition at 762 K. In the same way, for the temperature of 880 K, it has been calculated that the melt in which the initial mass fraction of $NaNO_2$ is 14.5 wt% shows the best thermal stability with respect to NO_3^- decomposition and NO_2^- oxidation.

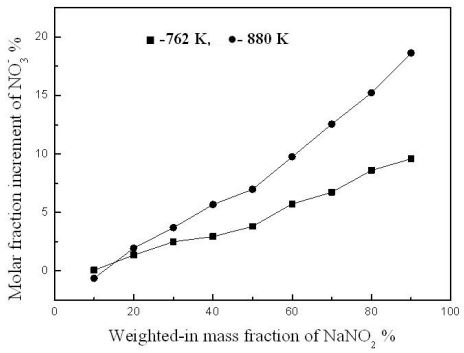

Fig. 6. Curve of molar fraction increment of NO_3^- versus initial mass fraction of $NaNO_2$ in KNO_3–$NaNO_2$ mixture.

In conclusion, concentration of NO_3^- and NO_2^- in molten KNO_3–$NaNO_2$ is analyzed by Raman spectroscopy, and the thermal stability under air atmosphere with respect to NO_3^- decomposition and NO_2^- oxidation is investigated.

After 30 min of holding time, the ions in the melts attain equilibrium, as the intensity ratio of characteristic bands between NO_3^- and NO_2^- is constant at 540 K and close to constant at 644 K.

When the temperature is lower than 644 K, concentration of NO_3^- in all of the molten samples remains almost the same for different temperatures. When the temperature is higher than 644 K, for the melts in which the initial concentration of KNO_3 is 90 wt%, the concentration of NO_3^- decreases a little with temperature. For the melts in which the initial concentration of KNO_3 is 10–80 wt%, the concentration of NO_3^- increases with temperature, and it increases more rapidly for lower initial concentration of KNO_3.

Molar fraction increment of NO_3^- changes due to high-temperature reaction and the equilibration increases linearly with the initial concentration of $NaNO_2$. The sample in which the initial fractions of $NaNO_2$ are 11.3 and 14.5 wt% exhibits the best thermal stability at 762 and 880 K, respectively with respect to NO_3^- decomposition and NO_2^- oxidation.

This work was financially supported by the National Natural Science Foundation of China (No. 51004034) and the Fundamental Research Funds for the Central Universities of China (No. N130402018).

References

1. T. Wang, D. Mantha, and R. G. Reddy, Appl. Energy **102,** 1422 (2013).
2. T. Wang, D. Mantha, and R. G. Reddy, in *Energy Technology 2012: Carbon Dioxide Management and Other Technologies*, M. D. Salazar-Villalpando, ed. (Wiley, HoBoken, 2012) p. 73.
3. S. Wright, T. Tran, C. Chen, R. Olivares, and S. Sun, in *Proceedings of Ninth International Conference on Molten Slags Fluxes and Salts* (2012).
4. R. G. Reddy, in *Proceedings of Ninth International Conference on Molten Slags, Fluxes and Salts* (2012).
5. J. Ding, Y. Chen, W. Chen, L. Hu, and G. Boulon, Chin. Opt. Lett. **10,** 071602 (2012).
6. S. Jin, C. Feng, Y. Jin, and Z. Zhang, Chin. Opt. Lett. **3,** 110666 (2005).
7. D. W. James and W. H. Leong, J. Chem. Phys. **49,** 5089 (1968).
8. D. W. James and W. H. Leong, J. Chem. Phys. **51,** 640 (1969).
9. D. W. James and W. H. Leong, Trans. Faraday Soc. **66,** 1948 (1970).
10. G. J. Janz and D. W. James, J. Chem. Phys. **35,** 739 (1961).
11. J. H. R. Clarke, Chem. Phys. Lett. **4,** 39 (1969).
12. K. Toshiko and T. Tohrc, Mol. Phys. **54,** 1393 (1985).
13. K. K. Sakai and T. Nakamura, Z. Naturf. **40,** 892 (1985).
14. C. W. Lieth and H. H. Eysel, J. Raman Spectrosc. **13,** 120 (1982).
15. R. W. Berg, D. H. Kerridge, and P. H. Larsen, J. Chem. Eng. Data **51,** 34 (2006).
16. B. L. Gao, F. G. Liu, Z. W. Wang, Z. N. Shi, X. W. Hu, X. X. Xue, and W. J. Gao, Rare Metals **28,** 581 (2009).
17. B. Gilbert and T. Materne, Appl. Spectrosc. **44,** 299 (1990).
18. E. Tixhon, E. Robert, and B. Gilbert, Appl. Spectrosc. **48,** 1477 (1994).
19. E. Tixhon, E. Robert, and B. Gilbert, Vib. Spectrosc. **13,** 91 (1996).
20. X. W. Hu, J. Y. Qu, B. L. Gao, Z. N. Shi, F. G. Liu, and Z. W. Wang, Trans. Nonferrous. Met. Soc. China **21,** 402 (2011).
21. R. I. Olivares, Sol. Energy **86,** 2576 (2012).
22. E. S. Freeman, J. Phys. Chem. **60,** 1487 (1956).
23. D. A. Nissen and D. E. Meeker, Inorg. Chem. **22,** 716 (1983).
24. C. Li, W. Lin, Y. Shao, and Y. Feng, Chin. Opt. Lett. **11,** 123001 (2013).
25. B. O. Mysen and J. D. Frantz, Contrib. Mineral. Petrol **117,** 1 (1994).
26. S. Gajaraj, C. Fan, M. Lin, and Z. Hu, Environ. Monit. Assess. **185,** 5673 (2013).